


# Current efficiency of individual electrodes in the sodium chlorate process: a pilot plant study

Kristoffer Hedenstedt<sup>1,2</sup> · Nina Simic<sup>1</sup> · Mats Wildlock<sup>1</sup> · Elisabet Ahlberg<sup>2</sup> 

Received: 17 March 2017 / Accepted: 14 June 2017 / Published online: 22 June 2017  
© The Author(s) 2017. This article is an open access publication

**Abstract** Current efficiency in the sodium chlorate process is a key issue in the evaluation of the power consumption. A pilot cell unit for executing the sodium chlorate process was constructed to study the current efficiency of the anode and cathode separately. The effects of sodium dichromate and sodium sulphate concentrations and the electrolyte temperature on the anode and cathode current efficiencies were studied. Corrosion products formed on the mild steel cathodes after their removal from the cell were characterised using X-ray diffraction and infrared spectroscopy. The results show that the cathodic current efficiency increases with increasing dichromate concentrations in the electrolyte until approximately  $5 \text{ g dm}^{-3}$  is reached. At this optimum concentration of dichromate, the presence of sulphate ions decreases the cathodic current efficiency. For moderate increases in temperature, the cathodic current

efficiency increases, but oxygen evolution is promoted, and the power consumption also increases. Surface characterisation of the electrodes after their exposure to air shows two primary types of behaviour, depending on the process parameters. At low dichromate concentrations, amorphous corrosion layers are formed, while at higher concentrations, reduced forms of iron hydroxides, i.e., “green rust”, are identified. Although the electrodes were positioned at the open circuit potential for 40 min before their removal from the cell, chromium remains on the cathode surface. This result might explain the corrosion-inhibiting effect of the addition of chromate to the electrolyte. The results from this study can be used to optimise operating procedures in real plants, decrease the energy consumption and minimise the environmental impact of these processes.

---

**Electronic supplementary material** The online version of this article (doi:[10.1007/s10800-017-1100-3](https://doi.org/10.1007/s10800-017-1100-3)) contains supplementary material, which is available to authorized users.

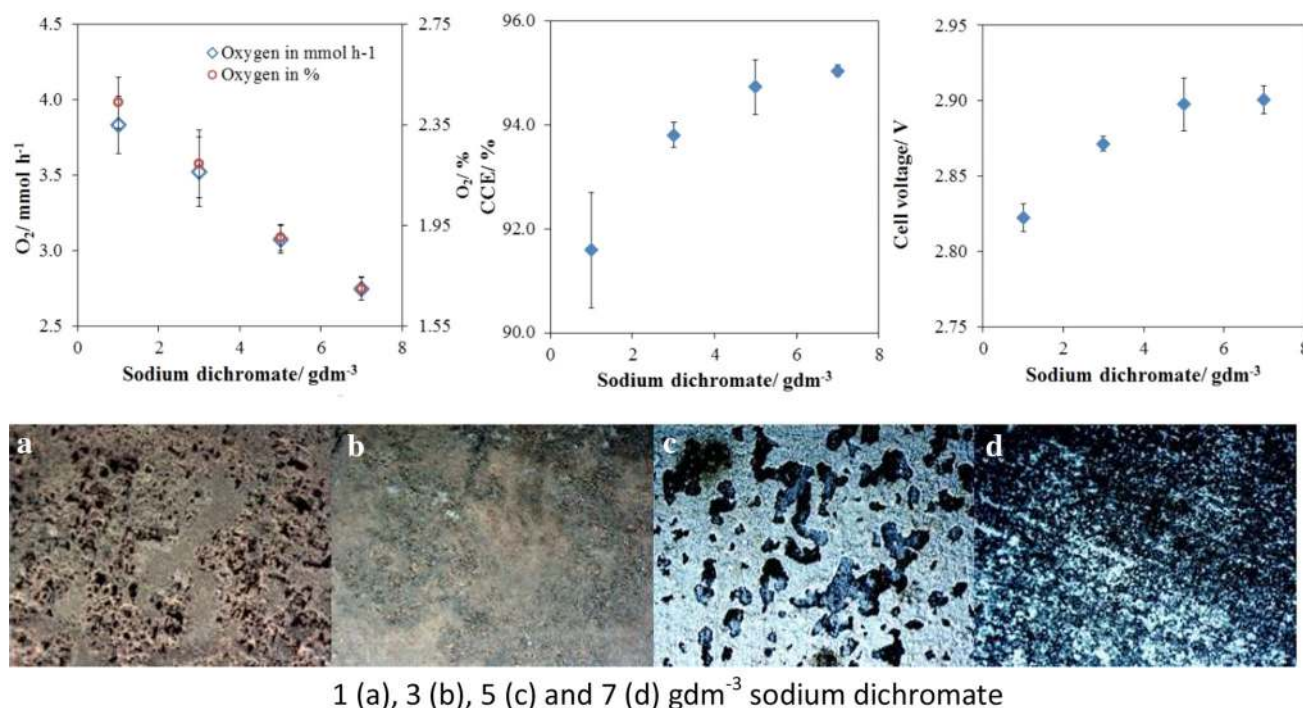
---

✉ Elisabet Ahlberg  
ela@chem.gu.se

<sup>1</sup> AkzoNobel Pulp and Performance Chemicals, 44580 Bohus, Sweden

<sup>2</sup> Department of Chemistry and Molecular Biology, University of Gothenburg, Kemigården 4, 41296 Gothenburg, Sweden

## Graphical Abstract



**Keywords** Pilot plant · Green rust · Chromate additions · Electrolysis · Surface characterisation · Temperature effect

## 1 Introduction

### 1.1 Background

The sodium chlorate process, with an annual production of approximately 3.6 million tons of NaClO<sub>3</sub> worldwide, is one of the most important electrolysis processes today. The process is quite energy intensive, with a power consumption of 4600–5000 kWh ton<sup>-1</sup> [1]. The main use of sodium chlorate is in the environmentally friendly elemental chlorine-free (ECF) bleaching of pulp. The sodium chlorate process has been developed for over more than one hundred years, but there are still opportunities for large energy savings by improving the selectivity and the cell potential.

Today, mild steel is the most frequently used cathode for the large-scale production of NaClO<sub>3</sub>, even though some plants are using titanium. Mild steel has been used since 1890, succeeding the previous graphite electrodes [2–4]. The material is cheap and has a fairly low overpotential for hydrogen evolution but suffers from low selectivity [5, 6]. A high faradaic yield is achieved by adding chromium (VI) to the electrolyte, which forms a Cr(III) film that provides high selectivity at the cathode [7]. A large drawback of the steel cathode is that it corrodes severely during the shut-down of the process, at which time the cathodic protection

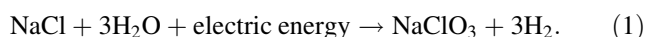
is lost. The corrosion process renders the need for a high concentration of chromate in the electrolyte and also a decreased current efficiency after the stop and during the build-up of the Cr(III) film [8].

The influence of different parameters, such as the addition of chromate, changing the temperature, the electrolyte concentration, the pH and the presence of additives, on the performance of the chlorate process has been reported [7–11]. The current efficiency has been studied in some publications, but the most common approach is to study the cell or electrode potential and oxygen production [9, 10, 12–17]. It has also been reported that the time it takes to reach stable conditions in a chlorate cell or at the surface of a chlorate cathode is significantly long [8]. The growth of the chromium (III) film on chromium and steel substrates was studied by Hamm, Olsson and Landolt [18]. They showed that an initial film grows within 10 s, depending on the conditions, while the formation of a fully developed film takes a much longer time. This report is supported by Ahlberg Tidblad et al., who showed that not even after 8000 s is a fully developed chromium (III) film established [19]. Several studies on the cathodic current efficiency, as related to the chlorate process, clearly show that the performance is time dependent. Directly after start-up, a quick and immediate increase in current efficiency is observed, followed by a slow increase in current efficiency until a final steady state far away from the timeline of most experiments is reached [8, 20, 21]. Hence, to achieve results that are relevant to full-scale conditions, it is of

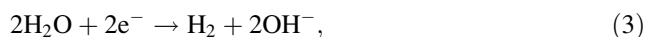
utmost importance to allow the system to reach the steady state in the study of the parameters. In the present study, this result has been achieved by using a pilot plant, running continuously for several days with planned stops. Different process conditions were evaluated with regard to performance, such as the temperature of the electrolyte, and the sodium dichromate and sodium sulphate concentrations in the electrolyte. In addition, a surface characterisation of the corrosion products formed on the cathodes was performed since it was shown in a recent study that two different types of iron oxyhydroxides found on chlorate cathodes actually influenced the time that was required to reach full current efficiency [17].

## 1.2 Current efficiency in the chlorate process: theory and practice

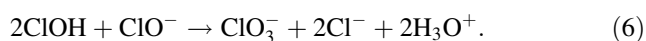
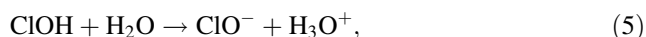
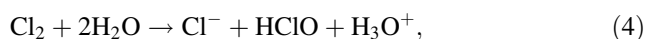
The true current efficiency is calculated from the amount of sodium chlorate formed in the electrolyte with respect to the amount of charge passed through the system. In full-scale production, this calculation is often done on a daily, weekly or monthly basis, and the time delay between the measurement of the added charge and the amount of chlorate is disregarded. A direct measurement is, however, slightly tedious and the chemical analysis of chlorate in combination with electrolyte volume measurements is needed. A more convenient way is an indirect method comprising the analysis of the gas production. This measurement can be made continuously and with high accuracy and repeatability. The method relates to the basic overall reaction (1):



The overall reaction (1) is a summation of five different reactions taking place in the chlorate cell, two of which are heterogeneous electron transfer reactions taking place at the electrodes,



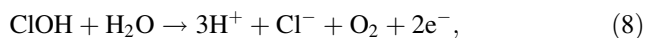
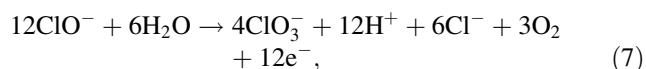
which are followed by three homogeneous chemical steps:



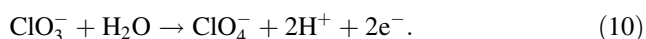
In the perfect process, the cell gas would consist of 100% hydrogen, and all electrons added would generate chlorate and hydrogen. However, several side reactions occur at the cathode that detract from hydrogen formation. At the anode and in the bulk, there are several side reactions that produce oxygen that mixes into the cell gas. The

benefit of using this method to measure the current efficiency is that it makes it possible to separate the different electrode processes and obtain the anodic, cathodic and total current efficiencies separately.

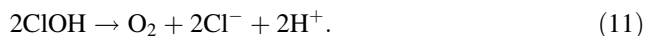
Almost all side reactions at the anode generate oxygen [9, 22, 23]:



By monitoring the oxygen formation in the cell gas, the anodic current efficiency can be calculated. However, there are some uncertainties in the coupling between the oxygen evolution and the efficiency. The anodic oxidation of chlorate to perchlorate does not form oxygen [24], but it is kinetically hindered and has a very low rate (reaction 10):

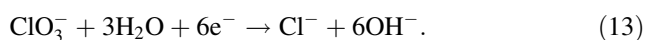
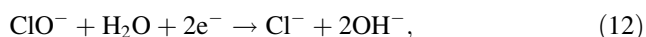


In the bulk electrolyte, homogenous hypochlorite decomposition occurs (reaction 11), giving rise to an anodic current efficiency (ACE) loss [9, 25]:



This is a redox reaction that causes the loss of the hypochlorite intermediate and the formation of oxygen. Recently, it was shown that the oxidation of hypochlorite ions is afflicted by excess oxygen evolution due to a radical mechanism induced by the first electron transfer step [23]. Despite the presence of these three reactions, measuring the oxygen content in the cell gas is considered to be an efficient way of obtaining the separate current efficiencies.

The main reaction at the cathode is hydrogen evolution, but two other reactions may occur that reduce the cathodic current efficiency (CCE) [5, 6]:



Based on reactions (12) and (13), the CCE can be calculated exclusively from the amount of hydrogen formed relative to the charge passed:

$$\text{CCE} = \frac{\tilde{n}\text{H}_{2\text{meas.}}}{\tilde{n}\text{H}_{2\text{theo.}}} = \frac{\tilde{n}\text{H}_{2\text{meas.}} 2F}{I}. \quad (14)$$

The anodic current efficiency can similarly be calculated from the oxygen content,

$$\text{ACE} = 1 - 2 \frac{\tilde{n}\text{O}_{2\text{meas.}}}{\tilde{n}\text{O}_{2\text{theo.}}} = 1 - 4 \frac{\tilde{n}\text{O}_{2\text{meas.}} F}{I}, \quad (15)$$

where  $\tilde{n}$  is the molar flow per second,  $F$  is the Faraday constant and  $I$  is the applied current. The total current efficiency is then the product of the individual parts.

## 2 Experimental

### 2.1 Testing equipment

Electrolytic testing equipment that accounts for the possibility for the long-term exposure of the electrodes under either potentiostatic or galvanostatic conditions in sodium chlorate electrolyte was designed for this work. The benefit of this equipment is that the performance/current efficiency of individual electrodes can be followed under different operating conditions, such as the presence of different additives and operation at different potentials and/or exposure times. The pilot plant was constructed as a combination of two parallel loops in which the first main loop was used to expose the electrodes to the electrolyte under constant conditions for up to 6 months. Located in parallel with the main loop, a second, considerably smaller, test loop was equipped with more instrumentation and gas analysis equipment for evaluating the current efficiencies. Through an extensive valve system, it is possible to switch an individual cell from the main loop to the test loop without breaking the polarisation of the electrodes. The electrolyte used in the test loop is taken from the main loop to maintain the same chemical composition. A schematic view is shown in Fig. 1.

The main loop reactor is a stirred jacketed titanium vessel of 200 dm<sup>3</sup>. The reactor is heated with a Lauda heating bath and has a propeller stirrer fitted into it. From the reactor, 1" titanium piping leads to four parallel mounted electrochemical cells. The cells used in the pilot plant, Fig. 2, have been developed at AkzoNobel Pulp and Performance Chemicals for the evaluation of electrode performance.

The cells were designed to simulate the electrolyte flow with a cell gap giving the same IR drop as in full scale. The fittings to the cells were made of PVDF and PTFE. The circulation of electrolyte was made possible by an ABB pump with a magnetic drive PVDF housing. A flow metre was used to control the flow in order to maintain a 0.5 ms<sup>-1</sup> laminar flow of the electrolyte over the electrodes. The pH was controlled in the loop with a Mettler

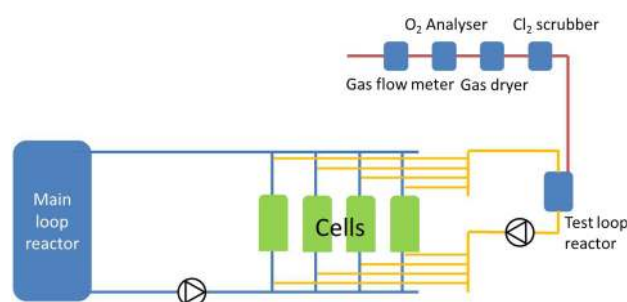


**Fig. 1** A schematic drawing of the test facility used in this project



**Fig. 2** Cutaway of the cells used in this work

Toledo InPro 4260i/SG pH electrode, and 2 M HCl was added to maintain a constant pH. An air flow of 3.6 m<sup>3</sup> h<sup>-1</sup> was purged into the reactor to dilute all formed hydrogen to a safe concentration that was well under the explosion limit. To compensate for evaporation, all gases were taken through a condenser and a level watch was connected to a pump to keep the level constant by the addition of deionised water. All four cells were connected individually to separate rectifiers with the ability to run in potentiostatic or galvanostatic modes.

With the extensive and intelligent valve system, each cell can be, by themselves or together, bypassed and put into the smaller test loop without cutting the load on the cells. The test loop has a 0.7 dm<sup>3</sup> jacketed glass reactor heated with a Lauda water bath. The pH was controlled in the same manner as in the main loop. Nitrogen can be added by either flushing large amounts of gas or controlling addition with a Brooks mass flow controller. The off gas was washed in 5 M NaOH to remove traces of chlorine and subsequently dried over silica gel. The clean and dry hydrogen and oxygen (and sometimes nitrogen) mixture was analysed for oxygen content by a Servomex paramagnetic oxygen analyser, and the total flow was measured by a Brooks mass flow metre. The combination of the mass flow of gas in normal ml min<sup>-1</sup> and the percentage of oxygen in the total flow were used to calculate the molar flows of oxygen and hydrogen so that current efficiencies could be estimated. The electrolyte circulation was generated by an Iwaki pump with PVDF housing generating 150 dm<sup>3</sup> h<sup>-1</sup>. In all investigations, the four different cells were tested to be able to get a mean value with errors.

#### 2.1.1 Validation of testing equipment

Stability tests and validation trials were made in the test pilot unit with titanium cathodes since they have proven to be stable and give high faradaic yields [20, 22]. The validation tests were run with four cells for 19 days with one power shutdown before the evaluation of the performance. The cathodic current efficiency was determined to be 97.2 ± 0.4% which is well in line with the work of Gustavsson et al. [20] as well as Spasojević et al. [7]. The cell voltage was 3.135 ± 0.015 V at a current density of 2 kA m<sup>-2</sup>. Variations of the individual electrode potentials were greater than for the cell voltage, indicating problems with the stability of the silver wire reference electrode over



time. Double reference electrodes were therefore connected afterwards for redundancy. When stable, the individual electrode potential was measured with an accuracy of  $\pm 18$  mV. Oxygen measurements showed a cell gas concentration of  $1.67 \pm 0.18\%$ , which resulted in a formation rate of  $1.67 \pm 0.18$  mmol h<sup>-1</sup>. These values closely correspond to what has been reported in the literature [7, 9, 26]. The results achieved in the validation trials closely resembles what can be found in the literature with respect to the cell potential, current efficiency and oxygen formation. Hence, the accuracy of measurements was found to be very good, and the estimated uncertainty of measurements given for each parameter was also considered to be within an acceptable range. The performance of the anode in the chlorate process varies over time, i.e., the initial performance during the “breaking-in period” and the final performance may differ [2, 27–30]. All tests were run with four different electrodes/cells to show repeatability and to obtain some statistics of the results such as mean values and standard deviations.

As the pilot was run unattended, it must be equipped with rigorous safety measures. The pilot used in the experiments had interlocks to avoid the explosive mixture of hydrogen and oxygen, as well as the incidental release of chlorine gas. These interlocks are mainly based on in-line measurements of potential, current, ventilation capacity, air purging, pH and flow measurements. Any event that can cause danger to a human or the environment will stop the equipment automatically; this is referred to as a ‘trip’.

### 2.1.2 Comparison between the pilot plant and full-scale plant performances

The performance of the pilot plant was validated against the full-scale plant performance. During the validation experiment, the pilot plant was run under constant conditions, and only the temperature varied (within 5 °C). The oxygen concentration and cell voltage were measured during the tests. For practical reasons, it was not possible to measure total current efficiency nor extract the cathodes for surface characterisation. The results from four different AkzoNobel sodium chlorate plants were used to span different cell technologies. Both monopolar and multi-monopolar cells were involved in the comparison. The temperature dependencies from the full-scale experiences at the four different plants show decreased cell gap voltages of 4–8 mV °C<sup>-1</sup> in the temperature interval of 70–80 °C. In the pilot study, the value in that interval showed a decrease of 6 mV °C<sup>-1</sup>. The correlation from this pilot study to the full scale is further exemplified by the temperature effect on the oxygen content; in the previously mentioned study, the four full-scale plants showed increased oxygen content in the off gas, with an average of

0.04–0.07% °C<sup>-1</sup>. The corresponding value in this pilot study is 0.05% °C<sup>-1</sup>.

## 2.2 Electrodes

DSA (PSC120 from Permascand) was used as the anode, and mild steel (DOMEX MS 21033 from SSAB) was used as the cathode; these electrodes were cut with a water jet and rinsed with deionised water. Aged steel cathodes from two different chlorate plants from AkzoNobel Pulp and Performance Chemicals were used in two test cycles. In one trial, cathodes made from titanium (grade 1 from Permascand) were used. The exposed electrode area in the test cells was 30 cm<sup>2</sup>. A simple Teflon-coated silver wire was used as the reference electrode (often referred to as a pseudo- or quasi-reference electrode) [31]. The silver wire was inserted into the centre of the cells and was made from pure silver wire from Sigma-Aldrich (99.9998%).

## 2.3 Chemicals

The electrolyte was produced from a brine of recrystallised NaCl and raw washed and dried NaClO<sub>3</sub> crystals from the AkzoNobel (Eka SC); the electrolyte was diluted to 110 g dm<sup>-3</sup> NaCl and 590 g dm<sup>-3</sup> NaClO<sub>3</sub> with deionised water. Sodium dichromate (Fluka, reagent grade) and sodium sulphate (Merck, p.a.) were added in appropriate amounts to fit the experiments. To maintain the pH in the electrolyte, NaOH and HCl (Scharlau p.a.) were added.

## 2.4 Method

Two different types of investigations were made. The first was a study of different process parameters on the fresh mild steel. Three different parameters were varied to investigate the effects on power consumption and corrosion. The parameters chosen were the temperature and the concentrations of sodium dichromate and sodium sulphate. These parameters were chosen since they are known to influence the performance of the process and are also simple to alter in the full-scale production. At the full scale, dichromate is added to improve the current efficiency and reduce corrosion in the process. The temperature is kept high to increase the conductivity and the reaction rates. Sodium sulphate enters the process as an impurity in the brine. It is not unusual to have concentrations up to 20 g dm<sup>-3</sup> of sodium sulphate in the electrolyte. In this study, the concentration of sodium dichromate was 1, 3, 5 and 7 g dm<sup>-3</sup>. In separate measurements, the sodium sulphate concentration was 0, 5, 10 and 20 g dm<sup>-3</sup>, while the sodium dichromate concentration was kept at 5 g dm<sup>-3</sup>. In the absence of sulphate and the presence of 5 g dm<sup>-3</sup> sodium dichromate, the temperatures studied were 65, 68,

71 and 78 °C. For each performance test, a fresh mild steel cathode was used and operated for several days. Plans were set to have only one controlled shutdown lasting 40 min every week, but the plant's own safety system did some emergency shutdowns due to various safety reasons marked as 'Trips' in Table 1. A schematic figure of the different trials is given in the supplementary information (Fig. S1).

#### 2.4.1 Stop procedure

Three different types of stops were made in the pilot during the investigations: intermediate stops, trips and final stops. Intermediate stops are made while the electrodes are connected to the main loop by shutting off the rectifier, i.e., the electrolyte flow and temperature are maintained. Thus, the corrosion occurs in the presence of a continuous supply of hypochlorite. Trips are unintentional stops triggered by the safety system. Two types of trips were observed in these experiments. The first type of trip was a shutdown of the rectifiers but with the heat and electrolyte circulation still running. The second type results in a complete electrical shutdown, meaning that the circulation and heating also stopped. During the trips, the electrodes were at open circuit potential and corrode in the electrolyte. The final stop was made when the electrodes were taken out of the main loop. Before the final stop, the cells were connected to the test loop, one-by-one, to measure the current efficiency, oxygen formation and cell voltage. Before the measurements were performed in the test loop, the system needed to reach the steady state. The reason was that the concentration of hypochlorite in the electrolyte would increase due to the lower electrolyte volume in the test loop relative to the applied current. There was also a delay in the gas monitoring system, as the test loop vessel was initially filled with nitrogen for safety reasons. Displacing the nitrogen and obtaining a stable hypochlorite concentration took a long time (2 h) for the first monitored cell, but then the system is equilibrated, and the following cells only needed 40 min to obtain stable values. An average of the measured values was taken during 15 min at the end of the time period. After the measurement, the electrode was reconnected to the main loop and the rectifier was stopped, i.e., the electrode was at the open circuit potential under the steady-state conditions in the main loop. The cathode underwent corrosion for 40 min, if not stated otherwise. The steady-state concentration of the sodium hypochlorite in the main loop was approximately  $0.5 \text{ g dm}^{-3}$ . During shutdown, the hypochlorite concentration decreases due to the chlorate formation reaction (6) and reaction in which it decomposes to oxygen (11). Approximately, 10–15 mol% decays during that 40 min, based on data obtained under very similar conditions reported by Cezner et al. [32]. After

the corrosion period, the electrolyte flow was stopped, the cell was emptied, and the electrode was removed and rinsed with deionised water. The removed electrodes were stored at ambient temperature in plastic bags in air. A summary of stops for the different tests is given in Table 1.

The second study was performed using cathodes that were previously used in two different chlorate plants. These electrodes were only run continuously, with no shutdown or trips during the test period. In this case, all electrodes were removed from the electrolyte while still polarised.

#### 2.5 Surface analysis

Photographs of the surfaces were taken through an Olympus stereo microscope at  $\times 20$  magnification. X-ray diffraction of the electrodes was made with a Siemens D5000 diffractometer with a  $\text{Cu K}\alpha$  ( $1.5418 \text{ \AA}$ ) radiation source at a  $5^\circ$  incidence angle. Fourier transform near infrared analysis was made in transmittance mode using KBr on a Nicolet 6700 FT-IR. Samples were prepared by cutting out coupons of  $2 \times 2 \text{ cm}$  for photographs and XRD analysis. For the IR measurements, the corrosion products on the coupons were scraped off from the coupon to be mixed with KBr for analysis. Energy dispersive X-ray analysis (EDX) was made with a Leo Ultra 55 FEG SEM equipped with an Oxford Inca EDX system. A 3 keV energy beam was used for imaging and 30 min of a 10 keV energy beam was used to perform the EDX analysis.

### 3 Results and discussion

#### 3.1 Implications of safety trips

The implications for corrosion and current efficiency from the described safety trips, Sects. 2.1 and 2.4.1, are difficult to estimate, as the plant started up, ran for several days afterwards and then stopped in a similar controlled manner for all samples. However, it is reasonable to believe that the time elapsed during the trip will influence the time for hypochlorite to oxidise the chromium (III) film as well as the steel cathode. There will most likely also be a difference in corrosion if the circulation is running during the trip or not. A continuous feed of hot hypochlorite-containing electrolyte should be more corrosive compared with the situation in which the circulation stops. Without the forced feed, the enclosed electrolyte in the cell gap will decrease in temperature and eventually be depleted of hypochlorite. The total exposure time for each electrode, as well as the intermediate, final stops and trips is given in Table 1. It is believed that the well-defined final step is decisive for the composition of the cathode.

**Table 1** Operation time and shutdown of the pilot plant during the trials. A trip is when the pilot unit shut down due to process safety issues or power failure

Na <sub>2</sub> Cr <sub>2</sub> O <sub>7</sub>	Days of trial	Intermediate stops	Trips	Final stop	Total stop time
1 g dm <sup>-3</sup>	8	–	1 × 19 h	80 min	20 h 20 min
3 g dm <sup>-3</sup>	14	–	1 × 34 h	40 min	34 h 40 min
5 g dm <sup>-3</sup>	14	1 × 40 min	–	40 min	1 h 20 min
7 g dm <sup>-3</sup>	15	1 × 40 min	–	40 min	1 h 20 min
Temperature	Days of trial	Intermediate stops	Trips	Final stop	Total stop time
65 °C	14	2 × 40 min	–	40 min	2 h
68 °C	14	1 × 40 min	–	40 min	1 h 20 min
71 °C	20	1 × 40 min	1 × 4 h <sup>a</sup>	40 min	5 h 20 min
78 °C	19	1 × 80 min	1 × 1.5 h	40 min	3 h 30 min
Na <sub>2</sub> SO <sub>4</sub>	Days of trial	Intermediate stops	Trips	Final stop, min	Total stop time
0 g dm <sup>-3</sup>	20	1 × 40 min	1 × 4 h <sup>a</sup>	40 min	5 h 20 min
5 g dm <sup>-3</sup>	20	1 × 40 min	2 h	40 min	3 h 20 min
10 g dm <sup>-3</sup>	20	2 × 40 min	–	40 min	2 h
20 g dm <sup>-3</sup>	22	1 × 40 min	1 × 15 min	40 min	1 h 35 min

<sup>a</sup> No circulation

### 3.2 Influence of sodium dichromate additions

#### 3.2.1 Process performance

The performance in the test loop was evaluated just before the final shutdown (see Sect. 2.4.1), and the values in Fig. 3 are the averages from four individual cells with their standard deviations shown as error bars. The rate of oxygen formation shows a linear decrease with the increase of sodium dichromate concentration in the electrolyte, Fig. 3a. Both cathodic current efficiency, Fig. 3b, and cell voltage, Fig. 3c, increase with the increasing content of sodium dichromate.

The rate of oxygen formation is presented as millimoles of formation per hour. The more commonly used unit, percentage of oxygen in cell gas, has been avoided since it can be misinterpreted when hydrogen gas formation varies, as noted by Hardee and Mitchel [9]. The experiments clearly show a linear trend of decreasing oxygen formation with the increasing concentration of dichromate in the electrolyte, Fig. 3a. This result is in line with full-scale plant experiences and other pilot trials, as discussed in the literature [9, 33]. In contrast, Hardee and Mitchel show in their experiments that the oxygen formation is constant with respect to the dichromate concentration in the range of 1–5 g dm<sup>-3</sup> [9]. However, their study used an electrolyte with only 50 g dm<sup>-3</sup> of NaCl, which gives unnaturally high oxygen content in the cell gas. Together with their claimed uncertainty in the measurements, it would not be possible to observe the same effect that is shown in the present work. The reason for the decrease in oxygen formation with increasing chromate concentration is due both

to the buffering effect of the chromate system, keeping the electrolyte pH in the optimal region for chlorate formation, and to the catalytic activity of chromium (VI) towards the disproportionation reaction of chlorate formation [7, 33–35]. Both of these phenomena keep the reactant (hypochlorite and hypochlorous acid) concentrations in the electrolyte low, which in turn lowers the possibility for oxygen formation, both in the bulk electrolyte (reaction 11) and at the anode (reaction 8). This is an indirectly positive effect of dichromate that needs to be considered if it is substituted with another substance.

The effect of chromate on the anode performance has been discussed in the literature. Cornell et al. [36] and Nylén et al. [37] discuss how the addition of chromate increases the buffer capacity and thereby hinders the decrease of the pH at the anode surface. They further discuss that the chromate adsorbed at the active sites leads to a higher overpotential, which in turn results in increased oxygen formation according to Eberil et al. [38]. However, in the present work, the total oxygen formation decreases with increasing chromate concentration, and thus, this effect must be very small compared with the catalytic effect of chromate on the disproportionation reaction.

The cathodic current efficiency is strongly dependent on the concentration of sodium dichromate in the electrolyte, as seen in Fig. 3b. The addition of sodium dichromate provides selectivity towards water reduction by forming a chromium (III) oxide or hydroxide that effectively blocks the reduction of hypochlorite and chlorate [16]. In addition to current efficiency, there are also a change in physical appearance as a result of the formation of the chromium

(III) film, i.e., the observable corrosion product and chromium (III) layer thickness.

### 3.2.2 Surface characterisation

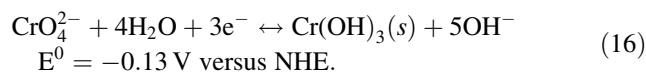
X-ray diffraction was used together with FTIR spectroscopy to analyse the corrosion products formed on the mild steel cathodes during the final stop. After removal of the electrodes from the main loop, they were rinsed with water and stored at ambient temperature in plastic bags in anticipation of surface characterisation. A first set of analyses was made using XRD and SEM/EDX after about three months.

A qualitative elemental analysis was made with EDX to get a rough view of the content at the surface. The surface layer contains mainly iron, chromium and oxygen but also, to a different degree, sodium, magnesium, calcium and chloride (Table 2).

The measurements show that chromium remains on the cathode surface even after spending a long time at the open circuit potential in the cell. It is generally believed that hypochlorite will oxidise the chromium film formed at the cathode during polarisation [8]. This belief is also supported from a thermodynamic point of view, as the oxidising power of hypochlorite is, by far and even at very low hypochlorite concentrations, enough to oxidise the chromium (III) film and the steel cathode. However, the experiments show that the chromium film lasts at least 40 min during shut-down. This persistence may well be the reason for its corrosion-inhibiting properties. The open circuit potential was also measured during shutdown for the planned stops, the trips and the final stops. In Fig. 4, the open circuit potential during the final stop is shown as a function of the dichromate concentration in the solution.

The open circuit potential reached a constant value between  $-0.2$  and  $-0.1$  V versus Ag/AgCl in the electrolyte. The potential of the Ag/AgCl electrode can be

estimated to  $E^0 = 0.169$  versus NHE at  $71^\circ\text{C}$  [39]. For oxidation of the chromium film, the redox reaction (16) applies:



At the pH of solution, 6.8, the potential for this reaction is approximately 0.45 V versus the reference electrode used in this study. It is clear that the chromium film is not oxidised under these conditions. The fairly constant potential that is obtained is probably related to the  $\text{Fe}(\text{OH})_3/\text{Fe}(\text{OH})_2$  redox couple in the solid phase ( $-0.35$  V vs. Ag/AgCl), which is slightly more negative than the measured potential. The measured open circuit potential is probably influenced by the presence of the hypochlorite/hypochlorous acid in the solution.

The iron content on the surface differs significantly between the samples and reflects the surface composition. With  $3 \text{ g dm}^{-3}$  of dichromate in solution, the iron content is approximately 20 at%, while at the higher concentrations of dichromate, it amounts to approximately 5 at%. Since the amount of chromium is fairly constant, this result indicates that the surface layer is much richer in iron with low dichromate concentrations in solution.

Further washing with water was performed, and new XRD and FTIR analyses were made. In general, the XRD spectra developed with time, showing more crystalline compounds on the surface. In Fig. 5, the results obtained after approximately one year are shown. The composition and amount of corrosion products on the cathode depend on the chromate concentration.

As the concentration of chromate in the solution increases, the corrosion products formed during shutdown become more crystalline (Fig. 5a). For the trials with 1 and  $3 \text{ g dm}^{-3}$  of sodium dichromate, the corrosion layer is mainly amorphous with some broad peaks in the XRD, indicating some ordering with small crystallites.

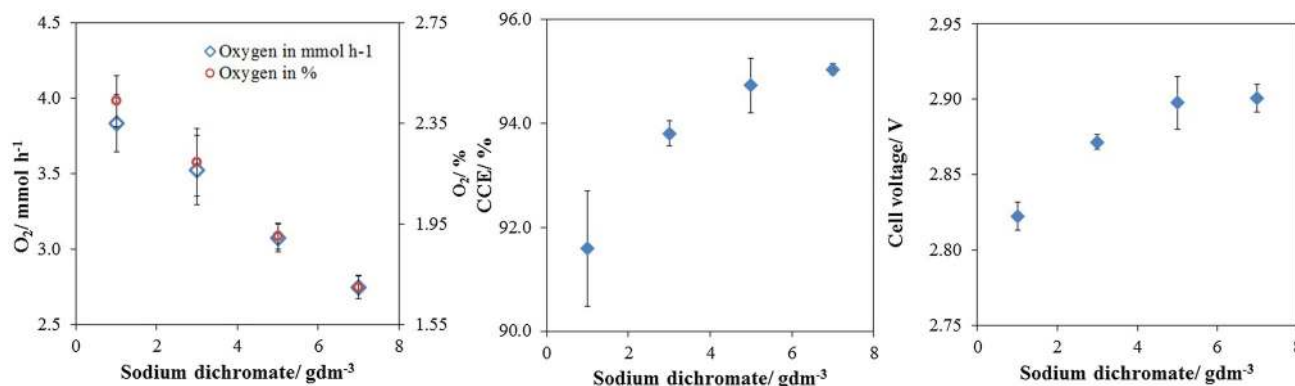


**Fig. 3** Measurements of the oxygen formation (a), cathodic current efficiency (b) and cell voltage (c) in a sodium chlorate pilot unit prior to the final stop. The electrolyte was  $110 \text{ g dm}^{-3}$  of NaCl,

$580 \text{ g dm}^{-3}$  of NaClO<sub>3</sub> and the concentration of sodium dichromate varied between 1 and  $7 \text{ g dm}^{-3}$  at  $71^\circ\text{C}$



Ferrihydrite is known to be poorly ordered, with two to six broad reflections in the XRD pattern, and might form on the surface. Ferrihydrite can be transformed into goethite and lepidocrocite depending on the conditions [40]. In the IR spectrum obtained with  $1 \text{ g dm}^{-3}$  of sodium dichromate (Fig. 5b), there are peaks at  $1020$ ,  $745$ ,  $610$  and  $478 \text{ cm}^{-1}$ , indicating the existence of lepidocrocite [40]. Peaks at  $890$  and  $796 \text{ cm}^{-1}$  are also observed that may arise from goethite [40]. In the trials at  $3 \text{ g dm}^{-3}$ , no lepidocrocite could be observed; rather, an oxidised form of green rust, exGR-Fe(III) [41], with broad peaks at  $655$  and  $470 \text{ cm}^{-1}$ , was found.

The two electrodes from the trials with  $5$  and  $7 \text{ g dm}^{-3}$  of sodium dichromate show similar results in the XRD and IR analysis [39]. First, it is evident that chlorate is left on the surfaces, even after a thorough rinsing in water. This presence is observed in both the XRD and IR (Fig. 5). In the IR spectra, the characteristic peaks for chlorate are marked with an \* (Fig. 5b). Green rust products are also observed: both green rust 1 (GR1), formed by inclusion of anions such as chloride and carbonate, and green rust 2 (GR2), containing three-dimensional anions such as sulphate or chromate. In the  $2\theta$  range used in XRD, the main peak for GR1 is located at  $\sim 11^\circ$ ; for GR2, the main peak is found at  $\sim 16^\circ$  with a smaller peak at  $\sim 24^\circ$ . Green rust has two characteristic peaks in the IR at  $\sim 420$  and  $550 \text{ cm}^{-1}$ , which are clearly observed in the IR spectra in Fig. 5b. Green rust products form by gentle oxidation of ferrous phases and are characterised by a crystal structure consisting of stacked brucite-like layers of  $\text{Fe}(\text{OH})_6$  octahedrons carrying positive charges and interlayers of anions and water molecules that restore the electroneutrality of the whole structure [41–47].

With higher concentrations of chromate in solution, the oxidation of the ferrous phases results in chloride-

**Table 2** The EDX analysis of surfaces with different amounts of sodium dichromate in the electrolyte

Element	at% $3 \text{ g dm}^{-3}$	at% $5 \text{ g dm}^{-3}$	at% $7 \text{ g dm}^{-3}$
Cr L	17.6	17.9	20.0
Fe L	20.5	4.8	5.6
O K	45.7	49.8	52.7
Cl K	0.8	5.7	2.4
Ag L	0.2	0.3	0.9
C K	10.8	8.9	7.5
Ca K	0.6	6.4	4.9
Mg K	1.0	2.2	3.1
Na K	0.7	1.8	1.1
Si K	1.1	0.3	0.3
Ti K	1.0	1.9	1.5

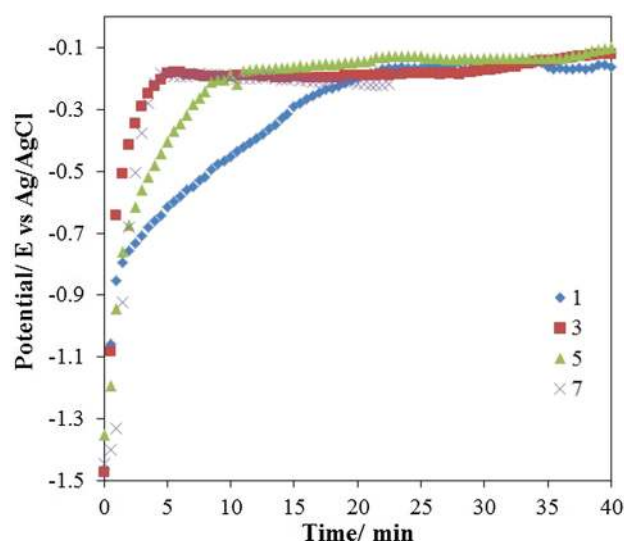


**Fig. 4** Open circuit potential on mild steel cathodes in sodium chlorate electrolyte after a shutdown of the process, with concentrations of sodium dichromate ranging from  $1$  to  $7 \text{ g dm}^{-3}$  in the electrolyte

containing GR1 and probably chromate or chromium (III) species in GR2. These GR products are surprisingly stable, since they were detected after storing the electrodes for one year in air. In the presence of sufficient amounts of chromate, the oxidation of ferrous phases may also involve the reduction of chromate, and the potential at the cathode remains low even in the presence of hypochlorite. It has been shown that chromium (III) species formed on the surface by subsequent oxidation of the ferrous iron inhibits the further oxidation of ferrous oxide [45]. This observation might explain the formation of green rust and the high amount of chromium found in the EDX analysis.

Hence, at low concentrations of sodium dichromate, the dominant corrosion product is a trivalent iron oxyhydroxide, while at high chromate concentrations, green rust is formed. Green rust has a lower oxidation state and is an intermediate in the oxidation of  $\text{Fe}(\text{OH})_2$  to different three-valent oxides or hydroxides [41, 48–50].

Lower amounts of corrosion products were formed on the cathode with increasing chromate concentrations in the electrolyte. This was visually seen in the photographs (Fig. 6 and especially in Fig. 6c, d) in which the grinding tracks are still observed. This result is due to the corrosion-inhibiting effect of the chromium (III) layer that is formed under cathodic polarisation [8, 9]. Also, the thickness of the chromium (III) film has been discussed in the literature as being beneficial for corrosion inhibition. It has been reported that the more chromate that is present in the electrolyte, the thicker the film gets [19]. However, from the cell voltage shown in Fig. 3c, it seems that the effect of the chromate levels off at concentrations approximately

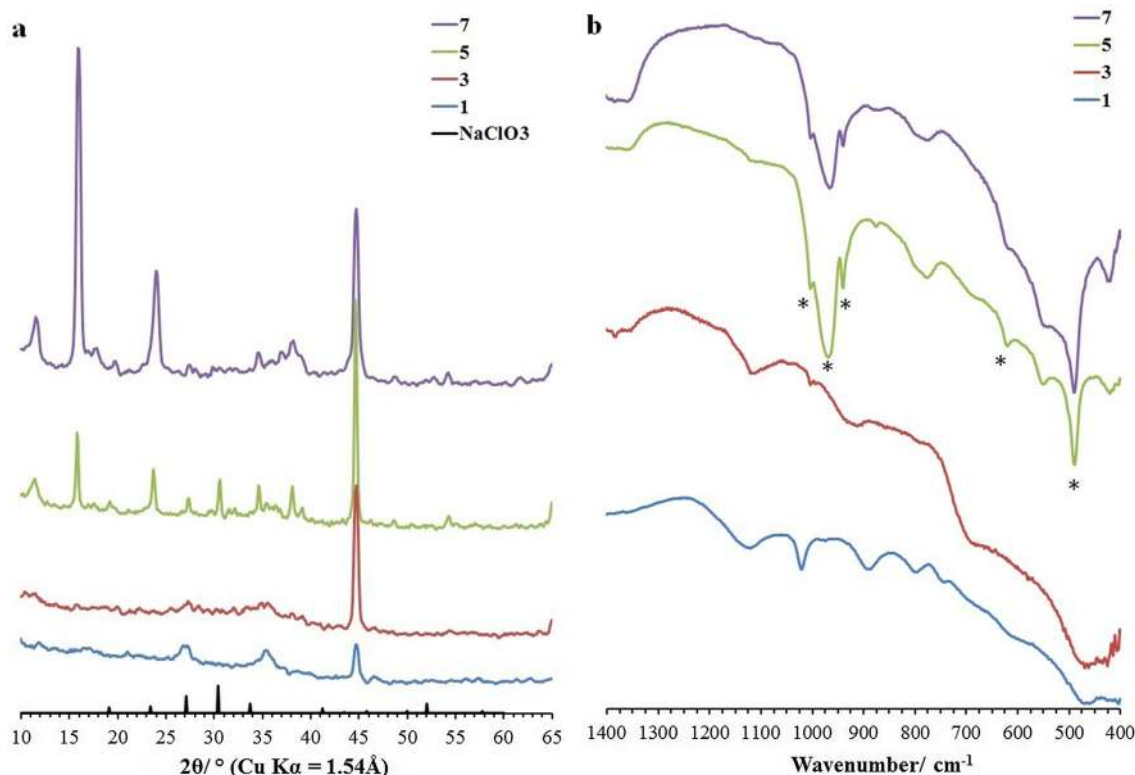


**Fig. 5** X-ray diffraction (a) and FT-IR transmission (b) analysis of corroded mild steel cathodes from pilot plant trials. The electrolyte was  $110 \text{ g dm}^{-3}$  of NaCl,  $580 \text{ g dm}^{-3}$  of  $\text{NaClO}_3$  and the levels of sodium dichromate varied between 1 and  $7 \text{ g dm}^{-3}$  at  $71^\circ\text{C}$ . The

reflection at  $44.7^\circ$  is related to the substrate. An XRD reference diffractogram is plotted from PDF 04-013-3719 and the asterisk represents the chlorate peaks in the IR spectrum

$5\text{--}7 \text{ g dm}^{-3}$ . This observation can be interpreted as a limiting thickness of the chromium layer, which is an interpretation supported by the work of Ahlberg Tidblad et al. [19].

The difference in corrosion products is also evidenced from the visual appearance of the electrodes, as their colours were divided into two sets. The electrodes subjected to 1 and  $3 \text{ g dm}^{-3}$  of chromate have an orange to dark brown colour, indicating iron (III) oxyhydroxides (Fig. 6a, b), while for the higher concentrations of sodium dichromate, 5 and  $7 \text{ g dm}^{-3}$ , the electrodes show a bluish green lustre (Fig. 6c, d), supporting the formation of green rust.

### 3.3 Temperature effects

#### 3.3.1 Process performance

The amount of oxygen in the cell gas (Fig. 7a) increases with increasing temperature. The cathodic current efficiency (Fig. 7b) increases with increasing temperature up to  $71^\circ\text{C}$ , followed by a dramatic decrease at higher temperatures. This effect is observed on all four cathodes investigated and is thus not an outlier. The cell voltages show a steady linear decrease with increasing temperature.

This is a good example of why the molar flow, rather than the percentage, of oxygen should be investigated. With the large variations in cathodic current efficiency, it would not have been possible to detect the almost linear response of oxygen formation to the temperature increase (Fig. 7a). The obtained temperature dependence of oxygen formation is in line with what Hardee et al. [9] have reported and discussed. The increase in oxygen formation relates to an increased decomposition rate of hypochlorite, as well as the oxidation on the anode described by reactions (7) or (8).

The cathodic current efficiency has also a clear temperature dependence. The current efficiency shown in Fig. 7b increases with the temperature from 65 to  $71^\circ\text{C}$ , while further increases in temperature lower the efficiency at the cathode. A possible reason for the decreased current efficiency at  $78^\circ\text{C}$  could be the reactions between the chlorate and the chromium (III) film. It has been shown earlier that chlorate can be reduced in the presence of chromium(III) at elevated temperatures [51].

The cell voltage decreases linearly by 83 mV from 65 to  $78^\circ\text{C}$ , Fig. 7c. The electrolyte conductivity changes, at the same time, from  $34.3 \text{ S m}^{-1}$  at  $65^\circ\text{C}$  to  $40.6 \text{ S m}^{-1}$  at  $78^\circ\text{C}$ . The cell voltage is thus reduced due to a decreased

iR drop of 36 mV under present conditions, which however, does not fully explain the entire voltage drop during the temperature increase. The remaining 47-mV decrease can be explained by effects at the electrodes, of which a 25-mV decrease was found on the anodic side (Fig. 8).

The magnitude of the decrease in anodic potential is in line with earlier studies [37]. The remaining potential dependence can be explained by effects at the cathode and are in the range of what has been reported earlier, 1.6–1.9 mV °C<sup>-1</sup> [10].

### 3.3.2 Surface characterisation

The XRD analysis (Fig. 9a) shows that at the lower temperatures, the phases have poor crystallinity. They resemble the XRD from the 1 and 3 g dm<sup>-3</sup> dichromate samples, with broad reflections at approximately 27° and 35°. The complementary IR spectra show small peaks that can be assigned to exGR-Fe(III). The XRDs from the electrode run at 71 °C have several reflections; the reflection at 2 $\theta$  equal to 19.1, 23.4, 27.1 and 30.4 can be assigned to sodium chlorate. This electrode has been rinsed but the removal of the chlorate was unsuccessful. It does also show a strong reflection at approximately 11° (GR1), as well as a small one at approximately 16° (GR2). The results are similar to the 5-g dm<sup>-3</sup> dichromate sample but with the opposite sizes of the reflections corresponding to GR1 and GR2. For the electrode exposed to 78 °C, the XRD reflections are again wider, showing poorly crystalline phases; however, GR1 and GR2 may still be seen in this surface.

In these trials, the colours of the electrodes were also divided into two sets. The electrodes from the lowest and highest temperatures, which also had the lowest current efficiencies, have an orange to dark brown colour (Fig. 10a, d), while those at the intermediate temperatures were blacker and blueish (Fig. 10b, c). Hence, electrodes exposed to the lowest and highest temperatures seem to have more of the trivalent corrosion product on the surface [40]. This indicates that the chromium (III) film found in the mid-temperature range protects the electrodes from the oxidising environment during a stop. This might be related

to decreasing the hypochlorite concentration with increasing temperature. However, as previously mentioned, at the high temperature the chlorate oxidation of the chromium(III) film becomes significant [51], resulting in more corrosion even though the hypochlorite concentration is lower.

## 3.4 Sulphate effects

### 3.4.1 Process performance

In the experiments where the sulphate concentration was varied, there is a decrease in the oxygen formation rate in the presence of sodium sulphate in the electrolyte (Fig. 11a). The rate of oxygen formation seems to exponentially decrease, but the order of magnitude on the error bars does give the impression of the formation being independent of sulphate concentration in the concentration range studied. In the literature, there are contradictory results [52–54] regarding the contribution of sulphate ions to the oxygen formation at the anode. Recently, Owe et al. showed that sulphate ions adsorb at the oxygen evolution active sites on iridium oxide electrodes [55, 56]. The cathodic current efficiency (Fig. 11b) is lower in the presence of sulphate but independent of concentration. The addition of sodium sulphate does not seem to affect the cell voltage since all of the values are within the standard deviation. However, an increase in the anode potential with sodium sulphate in the electrolyte has been reported by Nylén et al. [37]. According to the present results, such an increase in the overpotential must be compensated for by a lowering of the overpotential at the cathode, since the cell potential is the same in the absence and presence of sulphate ions in the electrolyte (Fig. 11c).

### 3.4.2 Surface characterisation

The experiment with 0 g dm<sup>-3</sup> of sulphate is the same as the experiment at 71 °C presented earlier. It shows GR1 and some GR2 on the surface, with chlorate potentially included in the structure. The two XRDs from samples 5 and 10 g dm<sup>-3</sup> of sulphate (Fig. 12a) did not show any

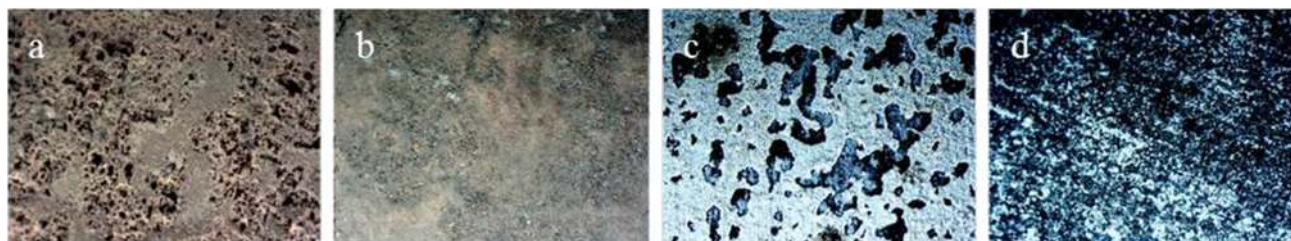


**Fig. 6** Photographs taken through an Olympus stereo microscope at  $\times 40$  magnification of corroded mild steel electrodes in electrolyte containing, from left to right, 1, 3, 5 and 7 g dm<sup>-3</sup> of Na<sub>2</sub>Cr<sub>2</sub>O<sub>7</sub>

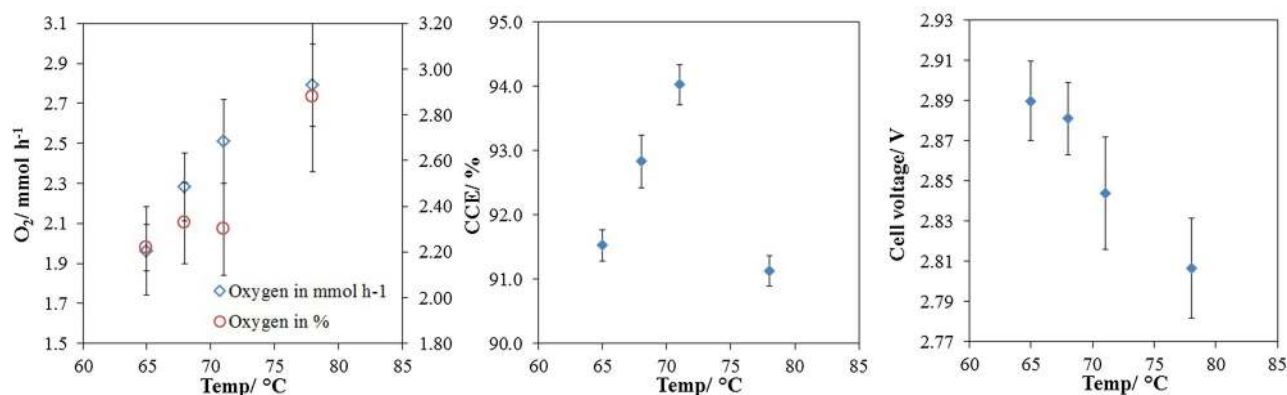


**Fig. 7** Measurements of the oxygen formation (a), cathodic current efficiency (b) and cell voltage (c) in a sodium chlorate pilot unit after two weeks of operation. The electrolyte was 110 g dm<sup>-3</sup> of NaCl,

580 g dm<sup>-3</sup> of NaClO<sub>3</sub>, and 5 g dm<sup>-3</sup> of Na<sub>2</sub>Cr<sub>2</sub>O<sub>7</sub>, and the temperature varied between 65 and 78 °C

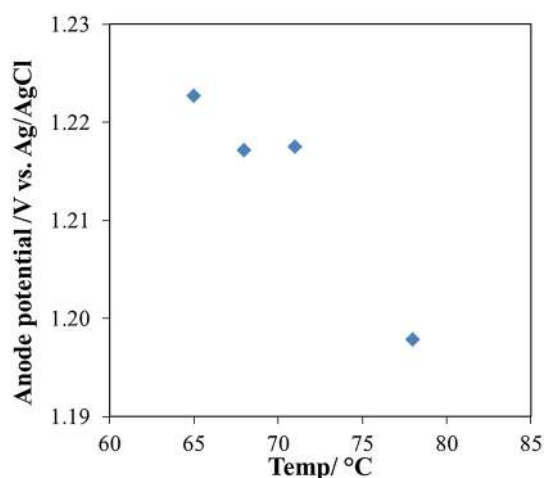


**Fig. 8** The anodic potential of the DSA electrode as a function of temperature at 2 kA m<sup>-2</sup>, pH 6.7, 110 g dm<sup>-3</sup> of NaCl, 580 g dm<sup>-3</sup> of NaClO<sub>3</sub> and 5 g dm<sup>-3</sup> of Na<sub>2</sub>Cr<sub>2</sub>O<sub>7</sub>

crystalline phases, just as was observed for the low temperature and low dichromate trials. The corresponding IR spectra (Fig. 12b) indicate that the corrosion layer consists of exGR-Fe(III). The XRD pattern from the electrode used at the highest concentration of sodium sulphate had several peaks related to GR2 and some small peaks related to GR1. Sodium chlorate was also present and was not removable with water. The IR spectra (Fig. 12b) show only exGR-Fe(III) for all electrodes.

The photographs taken of the electrodes (Fig. 13) show that for all electrodes with sulphate in the electrolyte (b, c and d), there are brown and blackish corrosion products on the surface. For the electrode without sulphate and with the highest current efficiency (Fig. 13a), the surface has a grey/bluish appearance. Hence, the sodium sulphate seems to increase the corrosion compared with the trials without sodium sulphate in the electrolyte. It seems that the

corrosion inhibition by the chromium (III) film is not sufficient when other species that promote the corrosion are present.

### 3.5 Electrodes previously used in sodium chlorate plants

To further relate the different corrosion products with the performance at full scale, two electrodes that have been in operation for several years in two different sodium chlorate plants, showing different performance levels, were investigated. The conditions during full-scale operation and the surface analysis of the electrodes have been described earlier [17].

The electrode from plant 1 had goethite on the surface, and the electrode from plant 2 had lepidocrocite. To show the differences in performance for these two iron oxyhydroxide species, they were tested in the pilot plant. The cathodic current efficiency as a function of time is shown in Fig. 14. The results clearly illustrate a large difference between the two corrosion products. For the electrode with goethite on the surface, the cathodic current efficiency is approximately 75% at the beginning and increases to approximately 90% during the time of experiment. In contrast, the current efficiency of the electrode with lepidocrocite on the surface is zero at the beginning and only slowly increases. After approximately 50 h, it performs similarly to the electrode with the goethite initially on its surface, and thereafter, the two electrodes have similar performance. These results clearly demonstrate that lepidocrocite initially inhibits the water reduction, which increases the power consumption and the cost of the process. The fact that the two different plant electrodes behave the same after approximately 50 h show that the active sites for hydrogen evolution are produced in the reduction process as described previously [15].



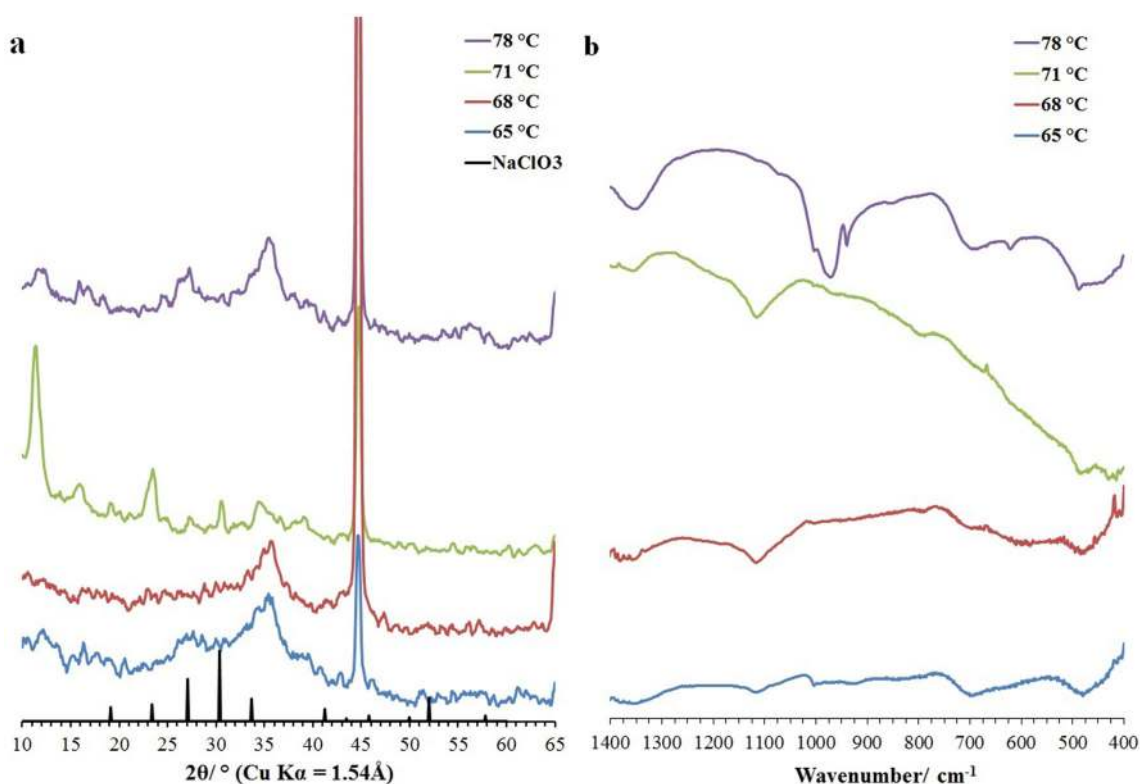


**Fig. 9** X-ray diffraction (a) and FT-IR transmission (b) analysis of corroded mild steel cathodes from pilot plant trials. The electrolyte was  $110 \text{ g dm}^{-3}$  of NaCl,  $580 \text{ g dm}^{-3}$  of  $\text{NaClO}_3$ , and  $5 \text{ g dm}^{-3}$  of  $\text{Na}_2\text{Cr}_2\text{O}_7$ , and the temperature varied between 65 and  $78^\circ\text{C}$ . The

reflection at  $2\Theta = 44.7$  is related to the substrate. An XRD reference diffractogram is plotted from PDF 04-013-3719 and the *asterisk* represents the chlorate peaks in the IR spectrum

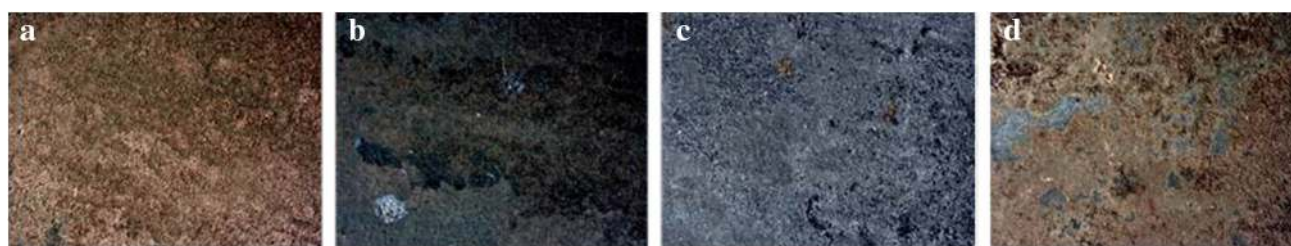


**Fig. 10** Photographs taken through an Olympus stereo microscope at  $\times 40$  magnification of corroded mild steel electrodes in electrolyte with a temperature of, from left to right, 65, 68, 71 and  $78^\circ\text{C}$

The IR spectra of the electrodes before they were tested in the pilot plant does show the characteristic peaks for goethite for the electrode from plant 1 and lepidocrocite for the electrode from plant 2 (Fig. 15). After the trials, the two electrodes showed similar structures. Peaks at  $800$  and  $795 \text{ cm}^{-1}$  for goethite and peaks at  $555$  and  $430$  for maghemite were apparent. No lepidocrocite could be detected on the electrode from plant 2. The XRD did not show conclusive results. Sharp peaks at  $2\Theta$  equal to  $31.7$  and  $45.5$  were observed for the electrode from plant 1, representing sodium chloride; peaks at  $23.4$ ,  $27.1$ ,  $30.4$  and

$33.7$ , representing sodium chlorate, could also be seen, but nothing more could be detected (Fig. 15).

From the photographs taken of the industrial electrodes, one can see that the cathode from plant 1 (Fig. 16a) has a colour between dark grey and black at the beginning. After the trial, the surface remained fairly similar, although the colour was a little bit more brownish (Fig. 16b). The cathode from plant 2 before the trial (Fig. 16c) had a colour between orange and brown on the surface; it is also the electrode with the low current efficiency at the beginning. After trials with the same stop procedure and running



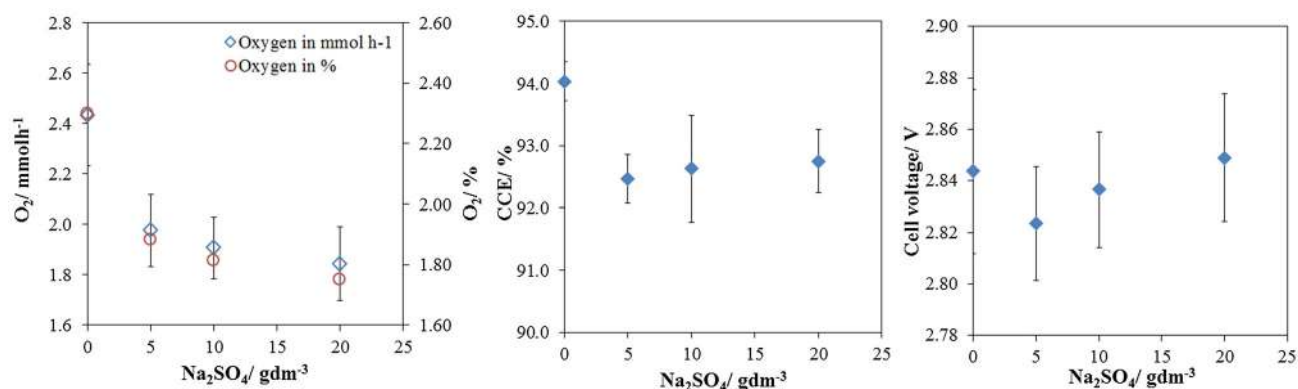


**Fig. 11** Measurements of the oxygen formation (a), cathodic current efficiency (b) and cell voltage (c) in a sodium chlorate pilot unit after two weeks of operation. The electrolyte was 110 g dm<sup>-3</sup> of NaCl,

580 g dm<sup>-3</sup> of NaClO<sub>3</sub>, and 5 g dm<sup>-3</sup> of Na<sub>2</sub>Cr<sub>2</sub>O<sub>7</sub> at 71 °C. Sodium sulphate was added to final concentrations of 0, 5, 10 and 20 g dm<sup>-3</sup>

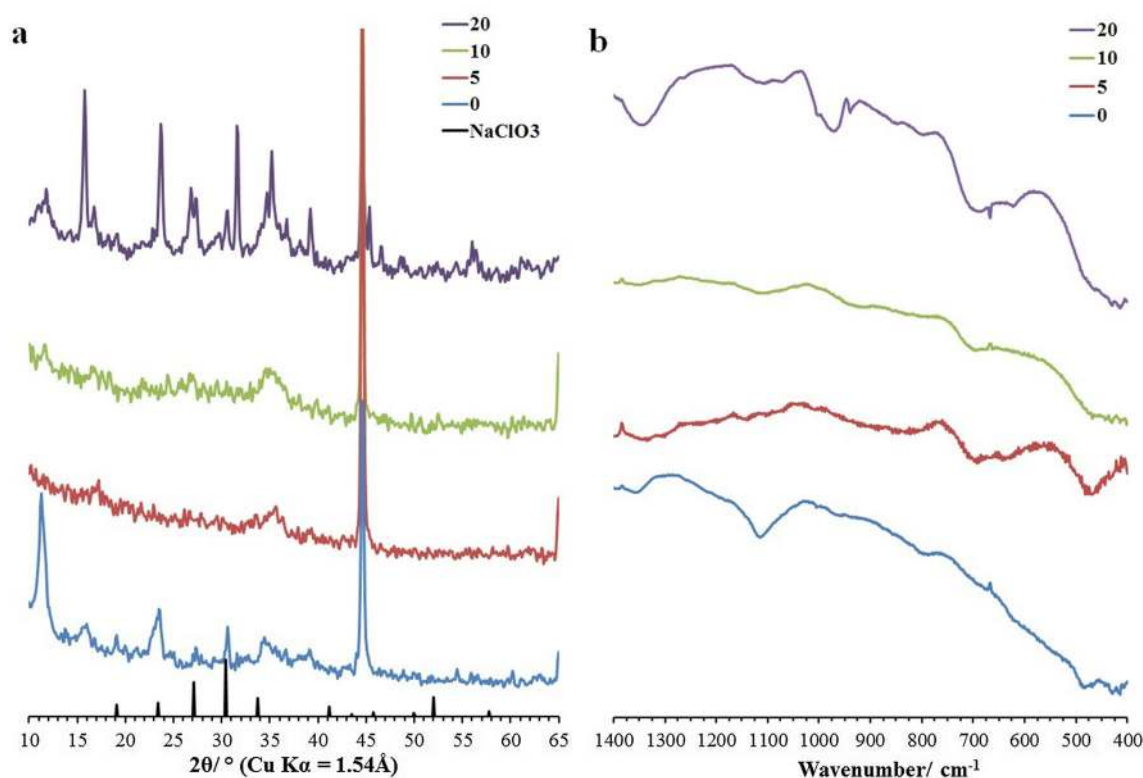


**Fig. 12** X-ray diffraction (a) and FT-IR transmission (b) analysis of corroded mild steel cathodes from pilot plant trials. The electrolyte was 110 g dm<sup>-3</sup> of NaCl, 580 g dm<sup>-3</sup> of NaClO<sub>3</sub>, and 5 g dm<sup>-3</sup> of

Na<sub>2</sub>Cr<sub>2</sub>O<sub>7</sub> at 71 °C. Sodium sulphate was added to final concentrations 0, 5, 10 and 20 g dm<sup>-3</sup>

conditions, as well as the same current efficiency, the visual appearances of the electrodes were the same (Fig. 16b, d). Hence, after reducing the corrosion product, the poorly performing (lepidocrocite) electrode was recovered. This result means that even though poor stop conditions may occur in the plants, it is not completely devastating for the cells. Running the plant under optimal conditions again will renew the surfaces and restore the good performance of the cathodes.

### 3.6 Power consumption

The increase in power consumption of poorly performing cathodes can be estimated from numeric integration of the current efficiency all the way to steady-state conditions. The steady state was considered to be achieved after 200 h. Adding the current efficiency to the formula for power consumption and multiplying with the production rate over

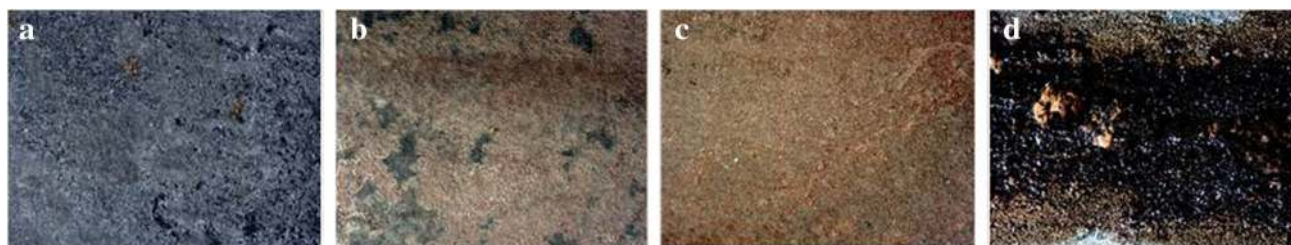


**Fig. 13** Photographs taken through an Olympus stereo microscope at  $\times 40$  magnification of corroded mild steel electrodes in electrolyte containing, from left to right, 0, 5, 10 and  $20 \text{ g dm}^{-3}$  of  $\text{Na}_2\text{SO}_4$

time will give the increase in kW h per start. The numeric integration was done as shown in the following equation:

$$\text{CCE}_{\text{avg}} = \frac{\int_0^{200} \text{CCE} dt}{\Delta t}, \quad (17)$$

where CCE stands for the cathodic current efficiency. This calculation yields an average cathodic current efficiency over the first 200 h. The power consumption,  $P$ , is calculated according to (17),

$$P = \frac{1511 U_{\text{cell}}}{\text{ACE} * \text{CCE}} [\text{kWh ton}^{-1}], \quad (18)$$

and the production rate at 100% current efficiency in the cell gap is

$$\text{Rate} = \frac{I3600M}{nF10^6} [\text{ton NaClO}_3 \text{ h}^{-1}], \quad (19)$$

where  $I$  is the current in Amperes,  $M$  is the molar mass in  $\text{g mol}^{-1}$ ,  $n$  is 6 electrons per chlorate molecule and  $F$  is the

Faraday constant. Combining these equations will give a value for the energy consumption during a start-up. The maximum of the measured CCE in this work was 94%, and this value can be used as a reference value to yield steady-state production costs. To find the costs for a start-up with a good cathode and a start-up with a poorly performing cathode, a couple of more values are needed. An average cell voltage of 2.8 V was found in this work, as well as an anodic current efficiency of 96%. The current running through the industrial cells was set to 70 kA, which is significant for the industrial cells of AkzoNobel, Atochem, Chemetics, and Krebs [57]. The figures quantifying the power consumption in one cell gap during 200 h of steady state operation, a start-up with a strongly performing cathode and a start-up with poorly performing cathode are seen in Table 3.

These values need to be multiplied by the number of cell gaps in a cell and the number of cells in a cell line to get the total energy cost for each start-up. For a contemporary plant with 50 thousand tons of annual production, each start-up with strongly performing cathodes will add 270,000 kW h; each start-up with poorly performing cathodes will add 351,000 kW h.

## 4 Conclusions

A pilot facility was used to investigate how different operating conditions in the sodium chlorate process affect the power consumption and, especially, the cathodic current efficiency and the corrosion of the cathodes. The results show the following:

The current efficiency of the cathodes increases with the increasing concentration of dichromate in the electrolyte, reaching a steady-state value approximately  $5$  to  $7 \text{ g dm}^{-3}$ .

The influence of sulphate in the electrolyte is negative for the cathodic current efficiency, but no concentration dependence could be determined.

There is an optimum temperature for the chlorate process at which the corrosion is minimised and the

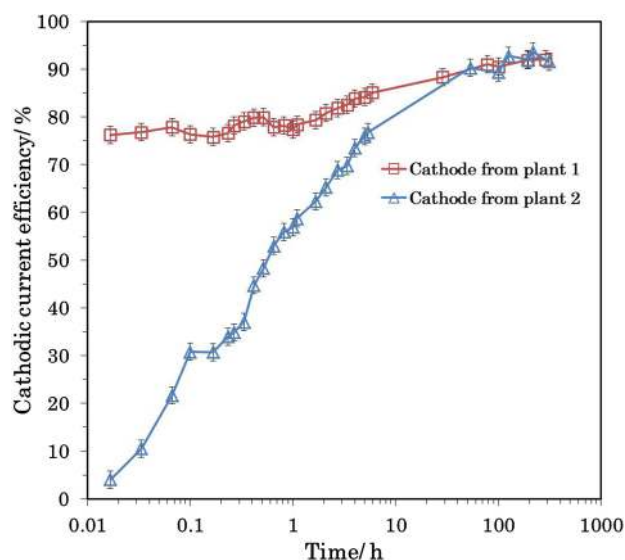


**Fig. 14** Pilot evaluation of used full-scale plant electrodes. The cathodic current efficiency is plotted for electrodes previously run in the sodium chlorate process. The surfaces of the electrodes consist of goethite ( $\alpha\text{-FeOOH}$ ) and lepidocrocite ( $\gamma\text{-FeOOH}$ ) [17]

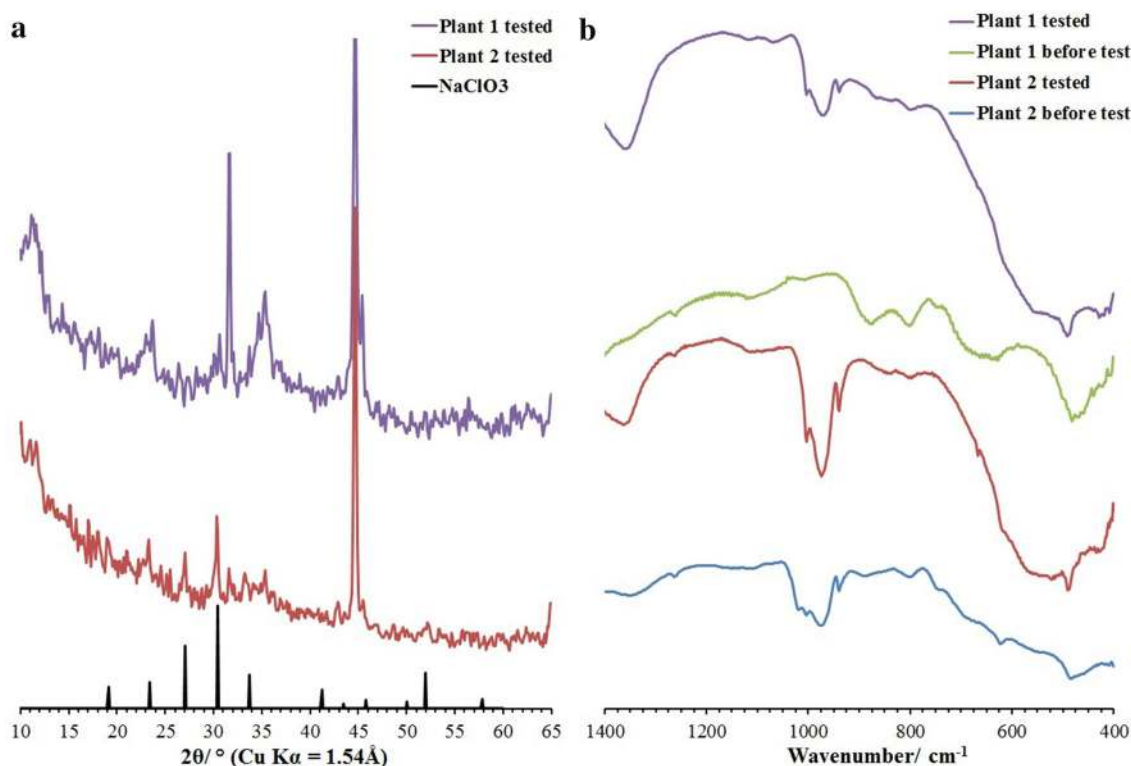


**Fig. 15** X-ray diffraction (a) and FT-IR transmission (b) analysis of corroded mild steel cathodes from pilot plant trials

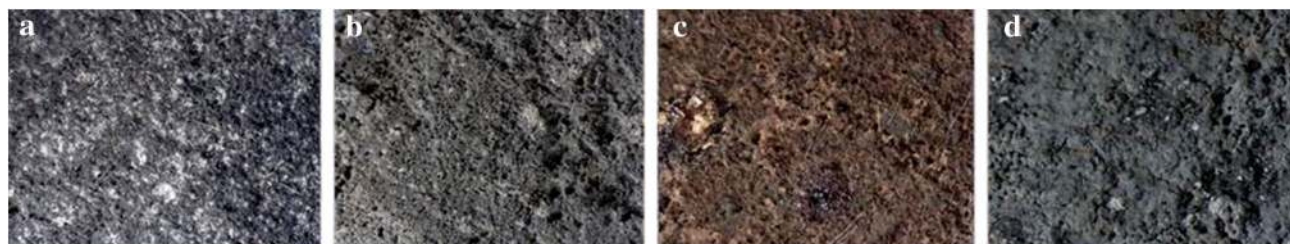


**Fig. 16** Photographs taken through an Olympus stereo microscope at  $\times 40$  magnification of corroded mild steel electrodes taken from, from *left to right*, plant 1 before the trial, plant 1 after the trial, plant 2 before the trial and plant 2 after the trial

**Table 3** Power consumption during start-up with steady-state performance, the use of good cathode and the use of poorly performing cathode for the production of sodium chlorate during 200 h at 70 kA, 2.8 V cell voltage and 96% anodic current efficiency

	Steady state/kWh	“Well performing cathode”/kWh	“Poorly performing Cathode”/kWh
Power consumption for 200 h per cell gap	43,400	45,400	46,000

cathodic current efficiency is maximised. Diversion from this value (approximately 71 °C) will decrease the current efficiency and increase the power consumption. Amorphous corrosion layers as well as “green rust” are found to be the most common corrosion species in these trials. This result is despite the fact that the electrodes were left at open circuit potential for 40 min before being taken out from the pilot cells.

It is remarkable that chromium stays on the surface of the cathode after shutdown and the subsequent corrosion period. The open circuit potential during shutdown indicates that iron corrodes, although the chromium (III) film remains under cathodic protection.

It is shown that if a poorly performing cathode is put into service under good conditions, it will slowly be regenerated and start to perform well again. This regeneration



period depends on the corrosion products that were formed on the cathodes.

**Acknowledgements** The authors would like to thank the Swedish Energy agency, 33280-1 and AkzoNobel Pulp and Performance Chemicals for financial support. Special gratitude is sent to the ones helping with the construction of the long-term test facility, Ulf Ahlgården, Johan Wanngård and Anders Amberntsson. We are also grateful for help in the management of the equipment and aid in the experiments provided by Annicka Sellin, Jan-Olof Johansson and Tobias Jonasson. A special thanks to Permascand for providing the electrodes.

**Open Access** This article is distributed under the terms of the Creative Commons Attribution 4.0 International License (<http://creativecommons.org/licenses/by/4.0/>), which permits unrestricted use, distribution, and reproduction in any medium, provided you give appropriate credit to the original author(s) and the source, provide a link to the Creative Commons license, and indicate if changes were made.

## References

- Cornell A (2014) Chlorate synthesis cells and technology. In: Kreysa G, Ota K-I, Savinell R (eds) Encyclopedia of applied electrochemistry, vol 1. Springer, New York, pp 181–187
- Cornell A (2014) Chlorate cathodes and electrode design. In: Kreysa G, Ota K-I, Savinell R (eds) Encyclopedia of applied electrochemistry, vol 1. Springer, New York, pp 175–181
- Viswanathan K, Tilak BV (1984) Chemical, electrochemical and technological aspects of sodium chlorate formation. *J Electrochem Soc* 131(7):1551–1559
- Carlson O (1890) SE-3614. Sätt att framställa underklorosyrliga och klorosyrade salter medelst elektrolys, Sweden Patent
- Taniguchi I, Sekine T (1975) The influence of chromate addition on the cathode reduction of hypochlorite ion. *Denki Kagaku* 43:201–208
- Lindbergh G, Simonsson D (1990) The effect of chromate addition on cathodic reduction of hypochlorite in hydroxide and chlorate solutions. *J Electrochem Soc* 137(10):3094–3099
- Spasojevic M, Krstajic NV, Jaksic JM (1984) Electrocatalytic optimization of faradaic yields in the chlorate cell process. *Surf Technol* 21:19–26
- Wulff J, Cornell A (2007) Cathodic current efficiency in the chlorate process. *J Appl Electrochem* 37:181–186. doi:10.1007/s10800-006-9263-3
- Hardee KL, Mitchell LK (1989) The influence of electrolyte parameter on the percent oxygen evolved from a chlorate cell. *J Electrochem Soc* 136(11):3314–3318
- Nylén L, Cornell A (2009) Effects of electrolyte parameters on the iron/steel cathode potential in the chlorate process. *J Appl Electrochem* 39(1):71–81. doi:10.1007/s10800-008-9642-z
- Jaksic M (1974) Mutual effect of current density, pH, temperature and hydrodynamic factors on current efficiency in the chlorate cell process. *J Electrochem Soc* 121(1):70–79
- Cornell A, Lindbergh G, Simonsson D (1992) The effect of addition of chromate on the hydrogen evolution reaction and on iron oxidation in hydroxide and chlorate solutions. *Electrochim Acta* 37(10):1873–1881
- Nylén L, Gustavsson J, Cornell A (2008) Cathodic reactions on an iron RDE in the presence of Y(III). *J Electrochem Soc* 155(10):E136–E142. doi:10.1149/1.2958299
- Lindbergh G, Simonsson D (1991) Inhibition of cathode reactions in sodium hydroxide solution containing chromate. *Electrochim Acta* 36(13):1985–1994
- Nylén L, Behm M, Cornell A, Lindbergh G (2007) Investigation of the oxygen evolving electrode in pH-neutral electrolytes: modelling and experiments of the RDE-cell. *Electrochim Acta* 52:4513–4524. doi:10.1016/j.electacta.2006.12.048
- Hedenstedt K, Gomes A, Busch M, Ahlberg E (2016) Study of hypochlorite reduction related to the sodium chlorate process. *Electrocatalysis* 7(4):326–335. doi:10.1007/s12678-016-0310-5
- Hedenstedt K, Simic N, Wildlock M, Ahlberg E (2016) Kinetic study of the hydrogen evolution reaction in slightly alkaline electrolyte on mild steel, goethite and lepidocrocite. *J Electroanal Chem* 783C:1–7. doi:10.1016/j.jelechem.2016.11.011
- Hamm D, Olsson C-OA, Landolt D (2002) Effect of chromium content and sweep rate on passive film growth on iron-chromium alloys studied by EQCM and XPS. *Corros Sci* 44:1009–1025
- Ahlberg Tidblad A, Mårtensson J (1996) In situ ellipsometric characterization of films formed by cathodic reduction of chromate. *Electrochim Acta* 42(3):389–398
- Gustavsson J, Li G, Hummelgård C, Bäckström J, Cornell A (2012) On the suppression of cathodic hypochlorite reduction by electrolyte additions of molybdate and chromate ions. *J Electrochem Sci Eng* 2:185–198. doi:10.5599/jese.2012.0021
- Gustavsson J, Nylén L, Cornell A (2010) Rare earth metal salts as potential alternatives to Cr(VI) in the chlorate process. *J Appl Electrochem* 40:1529–1536. doi:10.1007/s10800-010-0136-4
- Kotowskii S, Busse B, Wall K (1986) Modern chlor-alkali technology, vol 3. Ellis Horwood Ltd., Chichester, p 310
- Macounová KM, Simic N, Ahlberg E, Krtil P (2015) Electrochemical water-splitting based on hypochlorite oxidation. *J Am Chem Soc* 137(23):7262–7265. doi:10.1021/jacs.5b02087
- Tilak BV, Chen C-P (1999) Calculation of the current efficiency of the electrolytic sodium chlorate cell. *J Appl Electrochem* 29:1237–1240
- Hammar L, Wranglén G (1964) Cathodic and anodic efficiency losses in chlorate electrolysis. *Electrochim Acta* 9(1):1–16
- Colman JE (1981) Electrolytic production of sodium chlorate. *AIChE Symp Ser* 77:244–263
- Malmgren C, Eriksson AK, Cornell A, Bäckström J, Eriksson S, Olin H (2010) Nanocrystallinity in RuO<sub>2</sub> coatings—influence of precursor and preparation temperature. *Thin Solid Films* 518(14):3615–3618. doi:10.1016/j.tsf.2009.09.065
- Hummelgård C, Gustavsson J, Cornell A, Olin H, Bäckström J (2013) Spin coated titanium–ruthenium oxide thin films. *Thin Solid Films* 536:74–80. doi:10.1016/j.tsf.2013.03.044
- Cornell A, Håkansson B, Lindbergh G (2003) Ruthenium based DSA® in chlorate electrolysis—critical anode potential and reaction kinetics. *Electrochim Acta* 48(5):473–481. doi:10.1016/S0013-4686(02)00679-5
- Trasatti S (2000) Electrocatalysis: understanding the success of DSA®. *Electrochim Acta* 45(15–16):2377–2385. doi:10.1016/S0013-4686(00)00338-8
- Zhang X, Ju H, Wang J (2008) Electrochemical sensors, biosensors and their biomedical applications, 1st edn. Academic Press, New York
- Cezner V, Jaksic MM, Vlckova M, Mejta V, Rousar I (1990) Reactions in electrolyser for chlorate process. *Chem Biochem Eng Q* 4(2):83–92
- Wanngård J (2017) The catalyzing effect of chromate in the chlorate formation reaction. *Chem Eng Res Des.* doi:10.1016/j.cherd.2017.03.021
- Foerster F, Jorre F (1899) Zur Kenntniss der beziehungen der unterchlorigsauren salze zu den chloresäuren salzen. *J Pract Chem* 59:53–101

35. Müller E (1899) Über ein elektrlytisches verfahren zur gewinnung der chlor-, brom- und jodsuren salze der alkalien. *Zeitschrift für Elektrochemie* 41:469–473
36. Cornell A, Håkansson B, Lindbergh G (2003) Ruthenium-based dimensionally stable anode in chlorate electrolysis: effects of electrolyte composition on the anode potential. *J Electrochem Soc* 150(1):D6–D12. doi:[10.1149/1.1522386](https://doi.org/10.1149/1.1522386)
37. Nylén L, Cornell A (2006) Critical anode potential in the chlorate process. *J Electrochem Soc* 153(1):D14–D20. doi:[10.1149/1.2135216](https://doi.org/10.1149/1.2135216)
38. Eberil VI, Fedotova NS, Novikov EA, Mazanko AF (2000) Studying the link between the potential of a metal-oxide anode, the current efficiency for chlorate, and the current losses for the oxygen and chlorine evolution in a wide range of the chlorate electrolysis conditions. *Elektrokhimiya* 36(12):1463–1470
39. Greeley RS, Smith WT, Stoughton RW, Lietzke MH (1960) Electromotive force studies in aqueous solutions at elevated temperatures. I. The standard potential of the silver-silver chloride electrode. *J Phys Chem* 64:652–657
40. Schwertmann U, Cornell RM (2000) Iron oxides in the laboratory, 2nd edn. Wiley, New York
41. Legrand L, Mazerolles L, Chaussé A (2004) The oxidation of carbonate green rust into ferric phases: solid-state reaction or transformation via solution. *Geochim Cosmochim Acta* 68(17):3497–3507. doi:[10.1016/j.gca.2004.02.019](https://doi.org/10.1016/j.gca.2004.02.019)
42. Génin J-MR, Bourrié G, Trolard F, Abdelmoula M, Jaffrezic A, Refait P, Maitre V, Humbert B, Herbillon A (1998) Thermodynamic equilibria in aqueous suspensions of synthetic and natural Fe(II) – Fe(III) green rusts: occurrences of the mineral in hydromorphic soils. *Environ Sci Technol* 32(8):1058–1068. doi:[10.1021/es970547m](https://doi.org/10.1021/es970547m)
43. Peulon S, Legrand L, Antony H, Chaussé A (2003) Electrochemical deposition of thin films of green rusts 1 and 2 on inert gold substrate. *Electrochem Commun* 5(3):208–213. doi:[10.1016/S1388-2481\(03\)00019-5](https://doi.org/10.1016/S1388-2481(03)00019-5)
44. Génin J-MR, Ruby C, Upadhyay C (2006) Structure and thermodynamics of ferrous, stoichiometric and ferric oxyhydroxy-carbonate green rusts; redox flexibility and fougérite mineral. *Solid State Sci* 8(11):1330–1343. doi:[10.1016/j.solidstatesciences.2006.05.010](https://doi.org/10.1016/j.solidstatesciences.2006.05.010)
45. Skovbjerg LL, Stipp SLS, Utsunomiya S, Ewing RC (2006) The mechanisms of reduction of hexavalent chromium by green rust sodium sulphate: formation of Cr-goethite. *Geochim Cosmochim Acta* 70(14):3582–3592. doi:[10.1016/j.gca.2006.02.017](https://doi.org/10.1016/j.gca.2006.02.017)
46. Antony H, Legrand L, Chaussé A (2008) Carbonate and sulphate green rusts—mechanisms of oxidation and reduction. *Electrochim Acta* 53(24):7146–7156. doi:[10.1016/j.electacta.2008.05.008](https://doi.org/10.1016/j.electacta.2008.05.008)
47. Ahmed IAM, Benning LG, Kakonyi G, Sumoondur AD, Terrill NJ, Shaw S (2010) Formation of Green rust sulfate: a combined in situ time-resolved X-ray scattering and electrochemical study. *Langmuir* 26(9):6593–6603. doi:[10.1021/la903935j](https://doi.org/10.1021/la903935j)
48. Drissi SH, Refait P, Abdelmoula M, Génin JMR (1995) The preparation and thermodynamic properties of Fe(II)Fe(III) hydroxide-carbonate (green rust 1); Pourbaix diagram of iron in carbonate-containing aqueous media. *Corros Sci* 37(12):2025–2041. doi:[10.1016/0010-938X\(95\)00096-3](https://doi.org/10.1016/0010-938X(95)00096-3)
49. Olowe AA, Génin JMR (1991) The mechanism of oxidation of ferrous hydroxide in sulphated aqueous media: importance of the initial ratio of the reactants. *Corros Sci* 32(9):965–984. doi:[10.1016/0010-938X\(91\)90016-I](https://doi.org/10.1016/0010-938X(91)90016-I)
50. Jolivet JP, Chaneac C, Tronc E (2004) Iron oxide chemistry. From molecular clusters to extended solid networks. *Chem Commun* 5:481–487. doi:[10.1039/b304532n](https://doi.org/10.1039/b304532n)
51. Hedenstedt K, Edvinsson Albers R (2013) US 2013/0292261, Electrolytic process. US 2013/0292261 A1
52. Jaksic MM, Despic AR, Csonka IM, Nikolic BZ (1969) *J Electrochem Soc* 116(9):1316–1322
53. Bondar RU, Borisova AA, Kalinovskii EA (1974) Titanium-Ruthenium dioxide anodes in the electrolysis of chloride–sulfate solutions. *Elektrokhimiya* 10(1):44–48
54. Buné NY, Portnova MY, Filatov VP, Losev VV (1984) Effect of foreign anions on the kinetics of chlorine and oxygen evolution on ruthenium–titanium oxide anodes under the conditions of chlorine electrolysis. *Elektrokhimiya* 20(10):1193–1197
55. Owe L-E, Lervik IA, Tsyppkin M, Syre MV, Sunde S (2010) Electrochemical behavior of iridium oxide films in trifluoromethanesulfonic acid. *J Electrochem Soc* 157(11):B1719–B1725. doi:[10.1149/1.3490671](https://doi.org/10.1149/1.3490671)
56. Owe L-E, Tsyppkin M, Sunde S (2011) The effect of phosphate on iridium oxide electrochemistry. *Electrochim Acta* 58:231–237. doi:[10.1016/j.electacta.2011.09.043](https://doi.org/10.1016/j.electacta.2011.09.043)
57. Vogt H, Balej J, Bennet JE, Wintzer P, Sheikh SA, Gallone P, Vasudevan S, Pelin K (2010) Chlorine oxides and chlorine oxygen acids. *Ullman's Encycl Ind Chem*. doi:[10.1002/14356007.a06\\_483.pub2](https://doi.org/10.1002/14356007.a06_483.pub2)